



Enhanced trapping of Ni(II) ions by diatomite-supported nanoscale zerovalent iron from aqueous solution

Guodong Sheng^{a,b}, Xiangxian Ma^c, Wensheng Linghu^{b,*}, Zhongshan Chen^a, Jun Hu^d, Ahmed Alsaedi^e, Wafa Shammakh^e, Shatha Monaquel^e, Jiang Sheng^{f,*}

^aSchool of Chemistry and Environment, North China Electric Power University, Beijing 102206, China

^bCollege of Chemistry and Chemical Engineering, Shaoxing University, Zhejiang 312000, China, Fax: +86 575 8834 1521; email: wslinghu@usx.edu.cn

^cKey Laboratory of Petroleum Resources, Gansu 730000, China

^dSchool of Electronic Engineering, Dongguan University of Technology, Guangdong 523808, China

^eNAAM Research Group, Faculty of Science, King Abdulaziz University, Jeddah 21589, Saudi Arabia

^fNingbo Institute of Materials Technology & Engineering, Chinese Academy of Sciences, Ningbo 315201, China, email: shengjiang@nimte.ac.cn

Received 30 July 2016; Accepted 2 January 2017

ABSTRACT

This study investigated the effective trapping of Ni(II) ions by nanoscale zerovalent iron (NZVI) and diatomite-supported NZVI (NZVI-D) nanoparticles prepared via a borohydride reduction method. The confinement of iron crystal growth on the surface of diatomite leads to the formation of NZVI, resulting in the decreased aggregation and oxidation of iron nanoparticles, which can be proved by the analysis of structure, morphology and iron species. The batch experimental results indicated that the removal of Ni(II) by NZVI-D was higher than that by bare NZVI. Both the NZVI and NZVI-D displayed dual role namely adsorption and reduction during Ni(II) removal process. The presence of diatomite also improves the reducing capacity of NZVI by preventing agglomeration of NZVI, thus increasing its reactive surface area. This can be proved by the X-ray absorption fine structure analysis, which indicated that more Ni(II) ions can be reduced into Ni(0) by NZVI-D. This NZVI-D composite has potential applications in cleaning up environmental toxic metals like Ni(II) from wastewater.

Keywords: Nanoscale zerovalent iron; X-ray absorption fine structure; Diatomite; Ni(II) ions; Dual role

1. Introduction

Heavy metal ions are among the priority pollutants since they are not biodegradable, and consequently these metal ions can accumulate in the natural water or soil environment, which leads to the potential short-term and/or long-term hazards [1–5]. Among these metal ions, nickel (Ni(II)) ion has been widely used in stainless steel, manufacturing alloys, plating and so on, hence, the discharge of Ni(II) into the aqueous and/or soil systems will inevitably bring about various

detrimental effects on the natural ecology environment [1,5]. Therefore, it is very necessary to develop an effective method to treat Ni(II) and related heavy metal ions from wastewater. In this respect, zerovalent iron (ZVI) reduction has been regarded as an emerging environmental technology that is suggested to convey a cost-effective approach for the in situ and ex situ remediation of heavy metal-contaminated wastewater [1–4]. As a result, the ZVI material has been extensively accepted by various research groups as a versatile tool for the remediation of different kinds of environmental pollutants during the last decade [6–11]. By virtue of its lower particle size and higher surface area that brings about a high

* Corresponding author.

sequestration capacity, nanoscale zerovalent iron (NZVI) has receiving more and more attention for the sequestration of heavy metal ions like Ni(II), Zn(II), Cu(II), Cd(II), Co(II), Ag(I) and Pb(II), displaying that NZVI has larger sequestration capacity than conventional materials [1,12–16].

Despite of the wide applications of NZVI for immobilization of metal ions in water, challenges still remain in the real work of NZVI application, such as the aggregation of bare NZVI, resulting from a large surface area, which ultimately contributes to a decrease in NZVI reactivity [17]. Thus, to prevent the aggregation of NZVI and further improve the sequestration capacity of NZVI, strategies have been developed involving immobilization of NZVI on a suitable support, which can be used either as a carrier that is injected or as filling material in a reactive barrier [18]. Several different matrix supports have been utilized to immobilize NZVI, which included diatomite [18–20], layered double hydroxide [21–23], Mg(OH)₂ [24], rectorite [25], illite [26], montmorillonite [27], attapulgite [28], mesoporous silica [29] and carbon-based materials [30–33]. All these studies exhibited that the topic of metal ion retention by supported NZVI is an expanding area due to the decreased aggregation and increased reactivity of NZVI. Diatomite is naturally occurring, highly structured, fine hydrous silica that is formed from the remains of planktonic algae, which is also chemically inert and almost indestructible except in alkaline conditions. Therefore, the porous diatomite has been used in many applications due to its high surface area, high permeability and absorption, low bulk density and abrasion [18,34–37]. We used diatomite as a support of NZVI and found that diatomite showed multiple roles (enrichment of U(VI), pH buffering agent, scavenger for the insoluble reaction products during reaction) in NZVI interaction with U(VI) [20].

In the current study, we will extend the application of diatomite-supported NZVI (NZVI-D) in the immobilization of metal ions from wastewater. The trapping of Ni(II) on bare and supported NZVI will be studied and compared from a mechanistic view point. To our knowledge, no detailed study on the extent of Ni(II) uptake by supported NZVI at a molecule level is available in the literature.

2. Materials and methods

2.1. Chemicals and materials

All chemicals (like NaBH₄, FeSO₄·7H₂O, NiNO₃, NiO, Ni(OH)₂, NaOH, HCl) and commercial ZVI were purchased from Shanghai Chemical Co., China. The fraction of ZVI passing through a sieve of 0.15 mm was used for Ni(II) removal experiments. All solutions were prepared with 18 MΩ/cm high-purity water from a Millipore Milli-Q water purification system. The diatomite was obtained from Shengzhou County (Zhejiang, China). The raw diatomite was first physically purified in a centrifugal field to remove some impurities, then, the diatomite was processed by acid leaching in 1.0 mol/L HCl according to previous papers [19,20]. The NZVI was prepared by a chemical reduction approach. In brief, ~0.1 mol/L of NaBH₄ solution was slowly added into ~0.05 mol/L of FeSO₄ solution under continuous stirring, until the molar ratio [BH₄⁻]/[Fe²⁺] reached to be ~2.0. Then, the solution was stirred for another 30 min under room

temperature. The formed NZVI particles were settled and filtered, and then was washed with absolute ethanol for several times, and finally vacuum dried [20,38,39]. The NZVI-D was prepared by a similar chemical reduction approach for NZVI except that ~8.0 g of diatomite was uniformly mixed with FeSO₄ solution under continuous stirring before the addition of NaBH₄ solution. Before use, both NZVI and NZVI-D samples were stored in N₂ atmosphere to prevent atmospheric contamination and oxidation. The iron contents of the samples were measured to be 92.2% for ZVI, 54.7% for NZVI and 25.2% for NZVI-D using atomic absorption spectrometer [20].

2.2. Macroscopic and microscopic experiments

The macroscopic interaction experiments were carried out in a 150 mL conical flask containing the mixture of Ni(II) solution and different kinds of iron samples (ZVI, NZVI and NZVI-D). The Ni(II) solution was deoxygenated by N₂ stream before adding iron samples. The conical flask was sealed with a stopper during the entire experiment. Herein, a uniform dosage of iron was achieved by adding 0.0325 g of ZVI, 0.0548 g of NZVI and 0.1190 g of NZVI-D. The pH was adjusted to ~5.5 by adding negligible volume of 0.01 mol/L of HCl or NaOH. The reaction was conducted by putting the flask in a thermostatic shaker bath. At given time intervals, a series of mixture samples were withdrawn and filtered through a 0.22 μm membrane for determination of Ni(II) concentration by atomic absorption spectrometer (AA-6300C, Shimadzu, Japan). The removal of Ni(II) was calculated according to: removal (%) = (C₀ - C_e)/C₀ × 100%. The adsorption isotherms of Ni(II) onto diatomite were determined at various initial Ni(II) concentrations. All batch adsorption experiments were carried out in a thermostatic shaker bath. After equilibrium, the suspension was centrifuged for determination of Ni(II) concentration. The adsorbed capacity (q_e (mg/g)) was calculated: q_e (mg/g) = (C₀ - C_e) × V/m, where C₀ (mg/L) and C_e (mg/L) are initial and equilibrium concentration, respectively, V (mL) is the total volume and m (g) is adsorbent mass.

The microscopic information of the materials was characterized in detail by Mössbauer spectra (MBS) and X-ray absorption fine structure (XAFS). The MBS were measured at 290 K using a Bench MB-500 Mössbauer spectrometer and an X-ray source of 0.925 GBq ⁵⁷Co/Rh. The measured spectra were fitted to Lorentzian line shapes using standard line shape fitting routines. The half-width and peak intensities of the quadruple doublet were constrained to be equal. Isomer shifts were expressed with respect to the centroid of the spectrum of metallic iron foil (⁵⁶Fe > 99.85%). The XAFS at the Ni K-edge at 8,333 eV of the samples were recorded at room temperature in the fluorescent mode with silicon drift fluorescence detector at beam line BL14W1 of the Shanghai Synchrotron Radiation Facility (SSRF), China. The station was operated with an Si(111) double crystal monochromator. During the measurement, the synchrotron was operated at energy of 3.5 GeV and a current between 150 and 210 mA. The photon energy was calibrated with the first inflection point of Ni K-edge in Ni metal foil. Fluorescence spectra were collected using a multi-element pixel high purity Ge solid-state detector. Scans were collected in triplicate and averaged to improve the signal-to-noise ratio. Energy

calibration, fluorescence dead time correction and extended X-ray absorption fine structure (EXAFS) data analysis were performed with the SIXPack interface to the IFEFFIT package. EXAFS data reduction and linear combination fitting (LCF) analyses were performed using the following procedures. First, the averaged spectra were normalized with respect to E_0 determined from the second derivative of the raw spectra, and then the total atomic cross-sectional absorption was set to unity. A low-order polynomial function was fit to the pre-edge region and the post-edge region. Next, the data were converted from E -space to k -space and weighted by k^3 to compensate for dampening of the XAFS amplitude with increasing k space [5,31].

3. Results and discussion

3.1. Characterization of the materials

We can observe from the transmission electron microscope (TEM) image of the bare NZVI (Fig. 1(A)) that NZVI displayed as necklace-like aggregations because of the magnetostatic attraction between the iron particles. Whereas, we can observe from the TEM image of the NZVI-D (Fig. 1(B)) that NZVI particles were randomly distributed and well dispersed onto diatomite surfaces without clear aggregation, indicating that diatomite can weaken the aggregation effect of NZVI particles [20,38,39]. The X-ray diffraction patterns displayed that both NZVI and NZVI-D are mainly composed of ZVI (Fe^0) which could be characterized by the main peak at $\sim 44.5^\circ$ [20]. The specific surface areas of these materials were determined to be $26.1 \text{ m}^2/\text{g}$ for diatomite, $42.2 \text{ m}^2/\text{g}$ for NZVI, $29.5 \text{ m}^2/\text{g}$ for NZVI-D [20]. It was previously suggested that NZVI possess a typical “core-shell” structure that includes a core (i.e., ZVI and a shell (i.e., iron (hydr)oxides) [18,19]. So, the species of iron on both NZVI and NZVI-D samples were investigated

by ^{57}Fe MBS (Fig. 2), and the Mössbauer hyperfine parameters are shown in Table 1. We can see that all the Fe^0 , Fe^{2+} , Fe^{3+} species were present in both NZVI and NZVI-D samples. Nevertheless, the relative content of Fe^0 (96.8%) of NZVI-D sample is higher than that (90.0%) of NZVI sample, indicating that NZVI-D exhibited a good anti-oxidation performance.

3.2. Enhanced immobilization of Ni(II) by NZVI-D

The immobilization of Ni(II) by various reactive materials was shown in Fig. 3. It can be seen from Fig. 3 that Ni(II) immobilized by diatomite via a sorption process is $\sim 10.5\%$ after 120 min reaction. Besides, we can see that Ni(II) immobilized by ZVI via a reduction process is only $\sim 25.8\%$ after 120 min reaction, which is much lower than that ($\sim 42.7\%$) of Ni(II) immobilized by NZVI. This phenomenon is in good agreement with the result reported by Lowry and Johnson [40] that nanosized iron with larger specific surface area is more reactive than commercial micron-scale iron. In their report, Lowry and Johnson regarded that gas bubbles (likely H_2) could be generated in the NZVI system, the rapid formation of H_2 might enhance the performance of Ni(II) immobilization, while these gas bubbles could not be observed in the ZVI system, hence, Ni(II) immobilization onto NZVI can be enhanced [40]. Moreover, during the synthesis of NZVI via a NaBH_4 reduction process, the reduction product $\text{B}(\text{OH})_3$ is less soluble, thereby, a certain amount of $\text{B}(\text{OH})_3$ can remain on NZVI surfaces, which also plays a significant role in Ni(II) immobilization since a Fe-B-oxide or Fe-B alloy may be formed on the surfaces, leading to the changes of the electronic properties of the oxide shell [40]. In addition, Ni(II) immobilization by NZVI-D via a reduction process after 120 min reaction is $\sim 92.9\%$, which is higher than the sum of Ni(II) immobilization by NZVI reduction and diatomite adsorption, suggesting that the use of diatomite

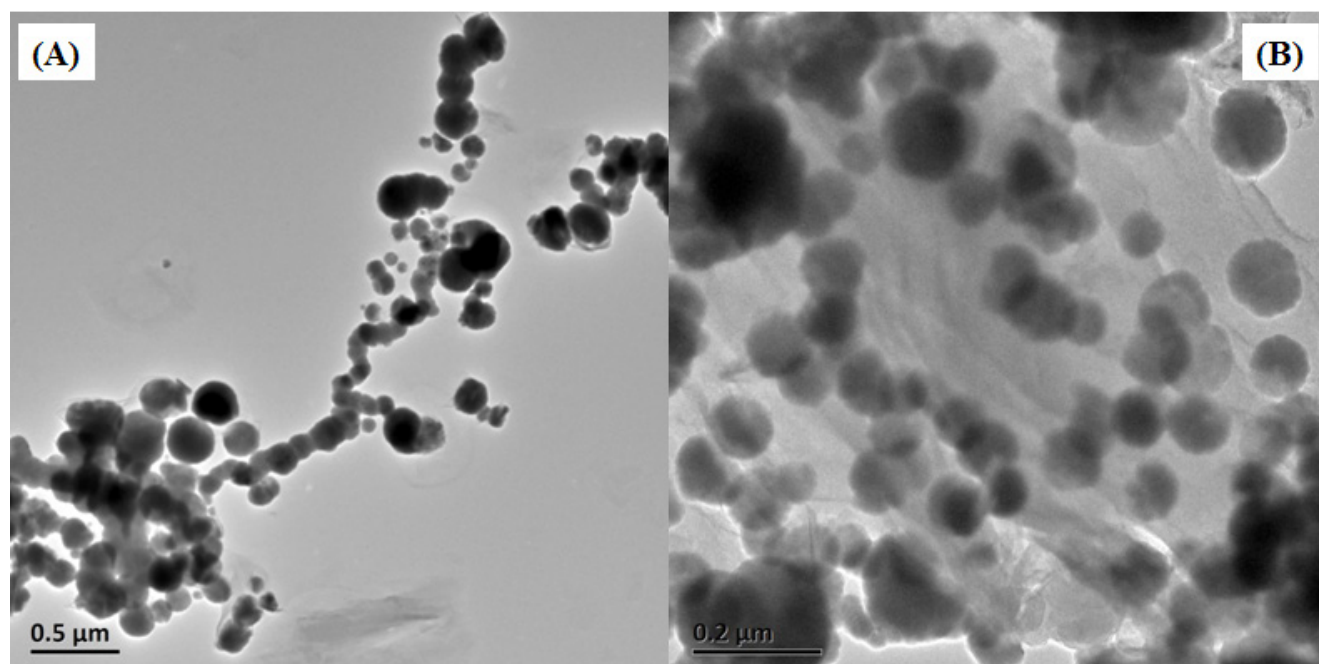


Fig. 1. TEM images of bare NZVI (A) and diatomite-supported NZVI (B).

to support NZVI may impose a good synergetic effect in the NZVI treatment system. Generally, immobilization of Ni(II) by NZVI is a surface-induced reduction reaction, therefore, the efficiency of Ni(II) immobilization is positively related to Ni(II) concentration on NZVI surface, namely, enrichment of

Ni(II) at the interface is an important process. The adsorption isotherm of Ni(II) on diatomite was shown in Fig. 4(A). The zeta potentials of diatomite as a function of pH were shown in Fig. 4(B). We can see that diatomite exhibits negative zeta potentials with pH ranging from 2.0 to 10.0, which is in favor of the adsorption of cationic Ni(II) ions. Therefore, in the NZVI-D treatment system, Ni(II) can more easily approach the reactive sites of NZVI due to the adsorption onto the negatively charged diatomite surfaces, resulting in the promotion of surface reaction. With more and more heavy metals released into the natural water and soil environment [41–45], the results do clearly demonstrate that the NZVI-D displayed a potential practical application as promising candidate in real work of environmental management.

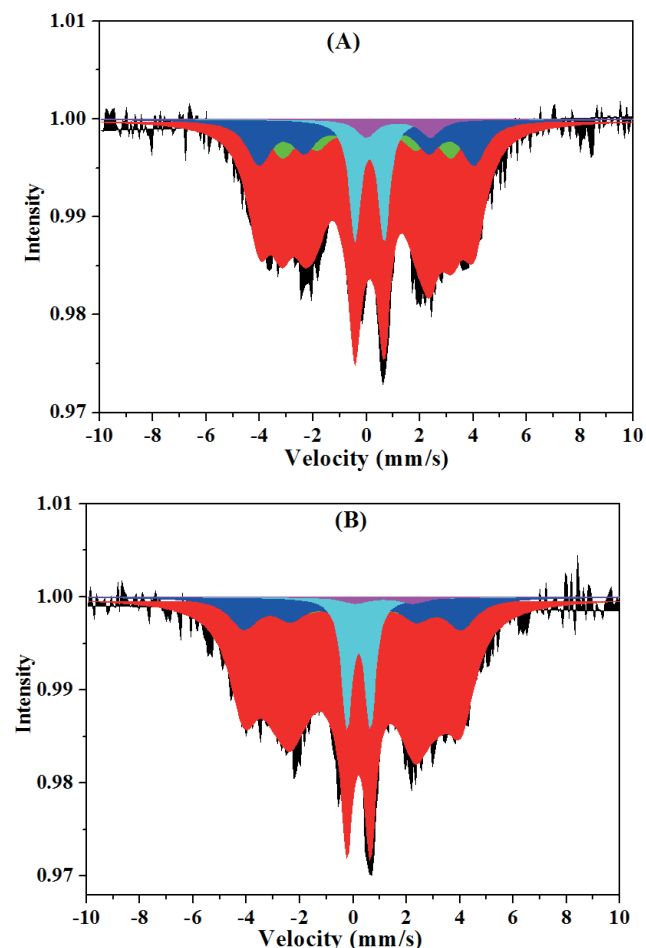


Fig. 2. ^{57}Fe Mössbauer spectra of bare NZVI (A) and diatomite-supported NZVI (B).

Table 1

Values of the hyperfine parameters from the best fits of ^{57}Fe Mössbauer spectra of bare NZVI and diatomite-supported NZVI

Samples	Iron species	Relative content (%)	IS (mm/s)	Q_s (mm/s)	HW (mm/s)	H_i (T)
Bare NZVI	Fe^0	40.64	0.005 ± 0.027	0.025 ± 0.049	0.554 ± 0.028	19.68 ± 0.299
	Fe^0	49.16	0.007 ± 0.021	0.007 ± 0.036	0.550 ± 0.021	24.98 ± 0.23
	Fe^{3+}	6.89	0.122 ± 0.011	1.097 ± 0.023	0.248 ± 0.018	
	Fe^{2+}	3.31	1.198 ± 0.060	2.400 ± 0.000	0.441 ± 0.113	
Diatomite-supported NZVI	Fe^0	41.05	0.051 ± 0.065	0.070 ± 0.136	0.853 ± 0.162	18.75 ± 0.889
	Fe^0	53.01	0.002 ± 0.027	-0.044 ± 0.047	0.657 ± 0.072	25.27 ± 0.32
	Fe^{3+}	4.86	0.211 ± 0.010	0.876 ± 0.021	0.223 ± 0.017	
	Fe^{2+}	1.07	1.170 ± 0.010	2.200 ± 0.000	0.575 ± 0.242	

Note: IS is the isomer shift (relative to $\alpha\text{-Fe}$ at room temperature), Q_s is the quadrupole splitting, HW is the half-width at half-maximum, H_i is the hyperfine magnetic field, relative content is the relative spectral absorption area for each species.

3.3. Effect of initial Ni(II) concentration on removal efficiency

The effect of initial Ni(II) concentration on removal efficiency in the NZVI-D treatment system was investigated in the range of 50–200 mg/L, and the results were shown in Fig. 5. Based on a previous research, Ni(II) removal by iron could be defined as a surface-mediated process, with more Ni(II) ions coming closely to iron, more iron can be oxidized

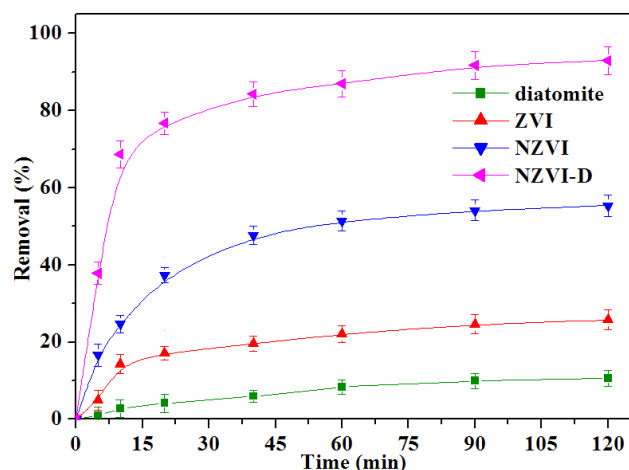


Fig. 3. Removal efficiencies of Ni(II) by various materials.

and lose their reactivity, leading to a decreased removal. In addition, the reaction products formed on iron surface will decrease the electron transfer from NZVI to Ni(II) and thus retard Ni(II) reduction [20]. Furthermore, for a fixed particle

dose, the total available reactive sites are limited for a reaction. So, the slower rate and lower efficiency of Ni(II) removal could be found at elevated concentrations of Ni(II). And the equilibrium time became longer as the initial concentration increased.

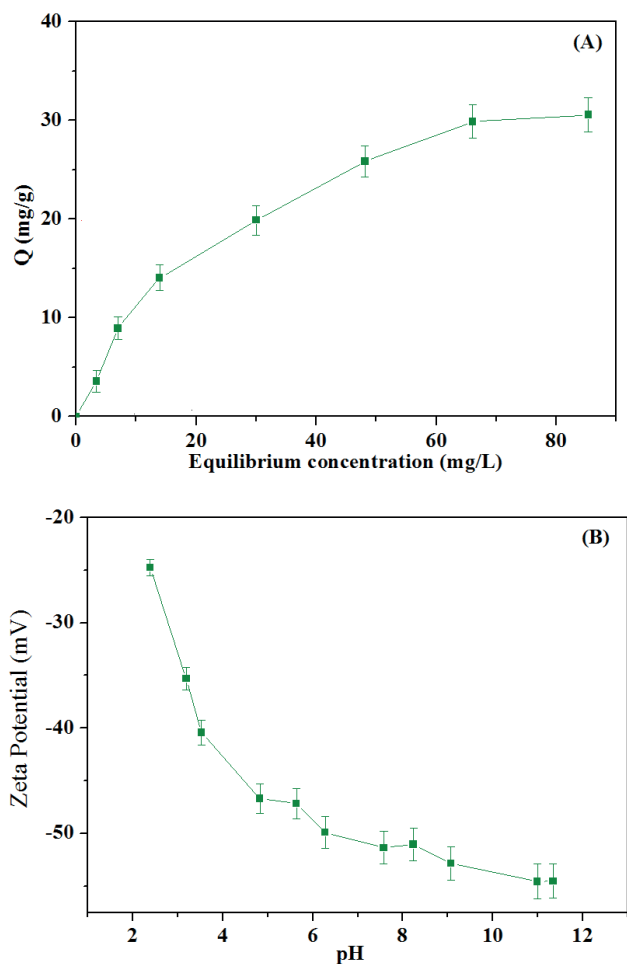


Fig. 4. (A) The adsorption isotherm of Ni(II) on diatomite and (B) zeta potentials of diatomite sample as a function of pH.

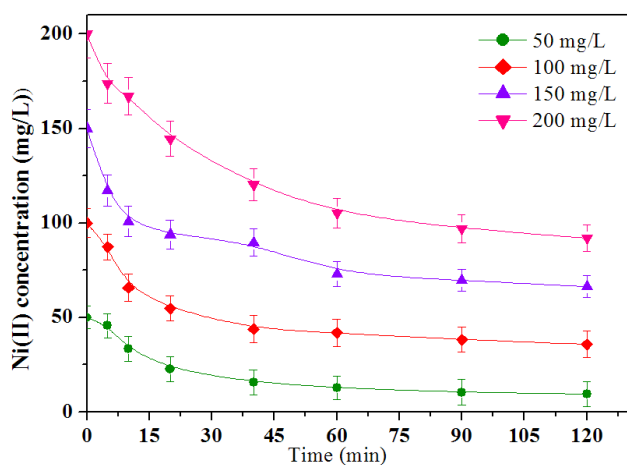


Fig. 5. Effect of initial concentration on the removal efficiency of Ni(II) in the NZVI-D treatment system.

3.4. Mechanistic aspects

The core-shell structure of NZVI enables them to show basically two mechanisms toward metal removal. Namely, the core that is constituted of Fe^0 forms an electron source that might reduce metal ions with a higher standard reduction potential than Fe^0 . While, the shell that possesses hydroxyl groups at the interface with solution is capable to trap metals by surface adsorption [1,13,14]. Previously, it was confirmed that the reduction potential of Ni(II) ions was more positive than Fe^0 , and Ni(II) was immobilized at NZVI surface by both sorption and reduction [13,14]. The EXAFS and LCF of NZVI and NZVI-D reaction with Ni(II) in water are shown in Fig. 6. We can see that 92.7% of Ni(II) and 7.3% of Ni(0) were present in NZVI sample after reaction, whereas, 85.2% of Ni(II) and

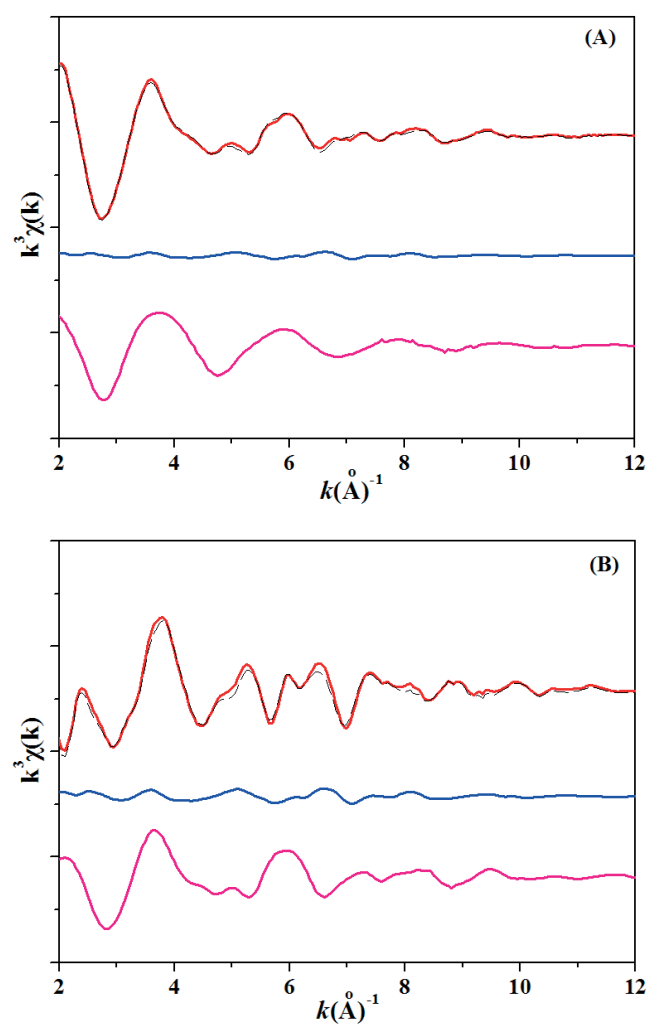


Fig. 6. The extended X-ray absorption fine structure (EXAFS) data and linear combination fitting (LCF) of NZVI (A) and NZVI-D reaction with Ni(II) in water.

14.8% of Ni(0) were present in NZVI-D sample. This result indicated that the reduction efficiency of NZVI increased utilizing diatomite as a support. Combined the results obtained herein and from previous reports [20,38,39], we could conclude that diatomite support played multiple roles including adsorbent of Ni(II), pH buffering effect, stabilizer and disperser of NZVI, as well as scavenger for insoluble reaction products during reaction. Namely, diatomite imposed an obvious synergistic effect in NZVI reaction system, which contributed to the enhanced reduction efficiency. The dual adsorption and reduction mechanisms on top of the large surface of nanoparticles produce rapid rate and high removal efficiency, offering NZVI and NZVI-D as efficient and promising materials for the immobilization of Ni(II) and related toxic heavy metals in environmental remediation.

4. Conclusions

The presence of diatomite during the synthesis of NZVI results in a partial decrease in their extent of aggregation, producing the characteristic core-shell structure. The NZVI-D particles demonstrated higher uptake capacities toward Ni(II) ions compared with bare NZVI. According to the XAFS results, NZVI ions were trapped through a dual adsorption and reduction mechanisms, which lead to the formation of Ni(II) surface complexes and to a lesser extent Ni(0). Besides, the reduction efficiency of NZVI increased when supported on diatomite.

Acknowledgment

This project was funded by the Deanship of Scientific Research (DSR), King Abdulaziz University, under grant no. 41-130-36-HiCi. The authors, therefore, acknowledge with thanks DSR technical and financial support.

References

- [1] N. Efecan, T. Shahwan, A.E. Eroğlu, I. Lieberwirth, Characterization of the uptake of aqueous Ni²⁺ ions on nanoparticles of zero-valent iron (nZVI), *Desalination*, 249 (2009) 1048–1054.
- [2] C. Ding, W. Cheng, Y. Sun, X. Wang, Effects of *Bacillus subtilis* on the reduction of U(VI) by nano-Fe⁰, *Geochim. Cosmochim. Acta*, 165 (2015) 86–107.
- [3] C. Tang, Y. Huang, Z. Zhang, J. Chen, H. Zeng, Y.H. Huang, Rapid removal of selenate in a zero-valent iron/Fe₃O₄/Fe²⁺ synergistic system, *Appl. Catal., B*, 184 (2016) 320–327.
- [4] C. Tang, Y.H. Huang, H. Zeng, Z. Zhang, Reductive removal of selenate by zero-valent iron: the roles of aqueous Fe²⁺ and corrosion products, and selenate removal mechanisms, *Water Res.*, 67 (2014) 166–274.
- [5] G. Sheng, S. Yang, J. Sheng, J. Hu, X. Tan, X. Wang, Macroscopic and microscopic investigation of Ni(II) sequestration on diatomite by batch, XPS and EXAFS techniques, *Environ. Sci. Technol.*, 45 (2011) 7718–7726.
- [6] L. Liang, W. Sun, X. Guan, Y. Huang, W. Choi, H. Bao, L. Li, Z. Jiang, Weak magnetic field significantly enhances selenite removal kinetics by zero valent iron, *Water Res.*, 49 (2014) 371–380.
- [7] X. Guan, Y. Sun, H. Qin, J. Li, I.M.C. Lo, D. He, H. Dong, The limitations of applying zero-valent iron technology in contaminants sequestration and the corresponding countermeasures: the development in zero-valent iron technology in the last two decades (1994–2014), *Water Res.*, 75 (2015) 224–248.
- [8] L. Liang, X. Guan, Z. Shi, J. Li, Y. Wu, P.G. Tratnyek, Coupled effects of aging and weak magnetic fields on sequestration of selenite by zero-valent iron, *Environ. Sci. Technol.*, 48 (2014) 6326–6334.
- [9] L. Liang, W. Yang, X. Guan, J. Li, Z. Xu, J. Wu, Y. Huang, X. Zhang, Kinetics and mechanisms of pH-dependent Se(IV) removal by zero valent iron, *Water Res.*, 47 (2013) 5846–5855.
- [10] Y.H. Huang, C. Tang, H. Zeng, Removing molybdate from water using a hybridized zero-valent iron/magnetite/Fe(II) treatment system, *Chem. Eng. J.*, 200–202 (2012) 257–263.
- [11] J. Li, H. Qin, X. Guan, Premagnetization for enhancing the reactivity of multiple zerovalent iron samples toward various contaminants, *Environ. Sci. Technol.*, 49 (2015) 14401–14408.
- [12] L. Ling, W. Zhang, Reactions of nanoscale zero-valent iron with Ni(II): three-dimensional tomography of the “hollow out” effect in a single nanoparticle, *Environ. Sci. Technol. Lett.*, 1 (2014) 209–213.
- [13] X.Q. Li, W.X. Zhang, Iron nanoparticles the core-shell structure and unique properties for Ni(II) sequestration, *Langmuir*, 22 (2006) 4638–4642.
- [14] X.Q. Li, W.X. Zhang, Sequestration of metal cations with zerovalent iron nanoparticles: a study with high resolution X-ray photoelectron spectroscopy (HR-XPS), *J. Phys. Chem. C*, 111 (2007) 6939–6946.
- [15] C. Uzum, T. Shahwan, A.E. Eroglu, I. Lieberwirth, T.B. Scott, K.R. Hallam, Application of zero-valent iron nanoparticles for the removal of aqueous Co²⁺ ions under various experimental conditions, *Chem. Eng. J.*, 144 (2008) 213–220.
- [16] O. Celebi, C. Uzum, T. Shahwan, H.N. Erten, A radiotracer study of the adsorption behavior of aqueous Ba²⁺ ions on nanoparticles of zero-valent iron, *J. Hazard. Mater.*, 148 (2007) 761–767.
- [17] T. Phenrat, N. Saleh, K. Sirk, R.D. Tilton, G.V. Lowry, Aggregation and sedimentation of aqueous nanoscale zerovalent iron dispersions, *Environ. Sci. Technol.*, 41 (2007) 284–290.
- [18] I. Dror, O. Jacov, A. Cortis, B. Berkowitz, Catalytic transformation of persistent contaminants using a new composite material based on nanosized zero-valent iron, *ACS Appl. Mater. Interfaces*, 4 (2012) 3416–3423.
- [19] Z. Sun, S. Zheng, G.A. Ayoko, R.L. Frost, Y. Xi, Degradation of simazine from aqueous solutions by diatomite-supported nanosized zero-valent iron composite materials, *J. Hazard. Mater.*, 263 (2013) 768–777.
- [20] G. Sheng, P. Yang, Y. Tang, Q. Hu, H. Li, X. Ren, B. Hu, X. Wang, Y. Huang, New insights into the primary roles of diatomite in the enhanced sequestration of UO₂²⁺ by zerovalent iron nanoparticles: an advanced approach utilizing XPS and EXAFS, *Appl. Catal., B*, 193 (2016) 189–197.
- [21] L. Shi, X. Zhang, Z. Chen, Removal of chromium(VI) from wastewater using bentonite-supported nanoscale zero-valent iron, *Water Res.*, 45 (2011) 886–892.
- [22] Y. Li, W. Cheng, G. Sheng, J. Li, H. Dong, Y. Chen, L. Zhu, Synergetic effect of a pillared bentonite support on Se(VI) removal by nanoscale zero valent iron, *Appl. Catal., B*, 174–175 (2015) 329–335.
- [23] L. Shi, Y. Lin, X. Zhang, Z. Chen, Synthesis, characterization and kinetics of bentonite supported nZVI for the removal of Cr(VI) from aqueous solution, *Chem. Eng. J.*, 171 (2011) 612–617.
- [24] M. Liu, Y. Wang, L. Chen, Y. Zhang, Z. Lin, Mg(OH)₂ supported nanoscale zero valent iron enhancing the removal of Pb(II) from aqueous solution, *ACS Appl. Mater. Interfaces*, 7 (2015) 7961–7969.
- [25] S. Luo, P. Qin, J. Shao, L. Peng, Q. Zeng, J.D. Gu, Synthesis of reactive nanoscale zero valent iron using rectorite supports and its application for orange II removal, *Chem. Eng. J.*, 223 (2013) 1–7.
- [26] C. Jing, Y. Li, R. Cui, J. Xu, Illite-supported nanoscale zero-valent iron for removal of ²³⁸U from aqueous solution: characterization, reactivity and mechanism, *J. Radioanal. Nucl. Chem.*, 304 (2015) 859–865.
- [27] J. Xu, Y. Li, C. Jing, H. Zhang, Y. Ning, Removal of uranium from aqueous solution using montmorillonite-supported nanoscale zero-valent iron, *J. Radioanal. Nucl. Chem.*, 299 (2014) 329–336.

- [28] Z. Liu, C. Gu, M. Ye, Y. Bian, Y. Cheng, F. Wang, X. Yang, Y. Song, X. Jiang, Debromination of polybrominated diphenyl ethers by attapulgite-supported Fe/Ni bimetallic nanoparticles: Influencing factors, kinetics and mechanism, *J. Hazard. Mater.*, 298 (2015) 328–337.
- [29] E. Petala, K. Dimos, A. Douvalis, T. Bakas, J. Tucek, R. Zboril, M. Karakassides, Nanoscale zero-valent iron supported on mesoporous silica: characterization and reactivity for Cr(VI) removal from aqueous solution, *J. Hazard. Mater.*, 261 (2013) 295–306.
- [30] G. Sheng, A. Alsaedi, W. Shammakh, S. Monaqueel, J. Sheng, X. Wang, H. Li, Y. Huang, Enhanced sequestration of selenite in water by nanoscale zero valent iron immobilization on carbon nanotubes by a combined batch, XPS and XAFS investigation, *Carbon*, 99 (2016) 123–130.
- [31] Y. Sun, C. Ding, W. Cheng, X. Wang, Simultaneous adsorption and reduction of U(VI) on reduced graphene oxide-supported nanoscale zerovalent iron, *J. Hazard. Mater.*, 280 (2014) 399–408.
- [32] X. Lv, J. Xu, G. Jiang, X. Xu, Removal of chromium(VI) from wastewater by nanoscale zero-valent iron particles supported on multiwalled carbon nanotubes, *Chemosphere*, 85 (2011) 1204–1209.
- [33] J. Li, C. Chen, R. Zhang, X. Wang, Nanoscale zero-valent iron particles supported on reduced graphene oxides by using a plasma technique and their application for removal of heavy-metal ions, *Chem. Asian J.*, 10 (2015) 1410–1417.
- [34] G. Sheng, R. Shen, H. Dong, Y. Li, Colloidal diatomite, radionickel, and humic substance interaction: a combined batch, XPS and EXAFS investigation, *Environ. Sci. Pollut. Res.*, 20 (2013) 3708–3717.
- [35] G. Sheng, S. Wang, J. Hu, Y. Lu, J. Li, Y. Dong, X. Wang, Adsorption of Pb(II) on diatomite as affected via aqueous solution chemistry and temperature, *Colloids Surf., A*, 339 (2009) 159–166.
- [36] G. Sheng, H. Dong, Y. Li, Characterization of diatomite and its application for the retention of radiocobalt: role of environmental parameters, *J. Environ. Radioact.* 113 (2012) 108–115.
- [37] G. Sheng, J. Hu, X. Wang, Sorption properties of Th(IV) on the raw diatomite-effects of contact time, pH, ionic strength and temperature, *Appl. Radiat. Isot.*, 66 (2008) 1313–1320.
- [38] G. Sheng, J. Hu, H. Li, J. Li, Y. Huang, Enhanced sequestration of Cr(VI) by nanoscale zero-valent iron supported on layered double hydroxide by batch and XAFS study, *Chemosphere*, 148 (2016) 227–232.
- [39] G. Sheng, Y. Tang, W. Linghu, L. Wang, J. Li, H. Li, X. Wang, Y. Huang, Enhanced immobilization of ReO_4^- by nanoscale zerovalent iron supported on layered double hydroxide via an advanced XAFS approach: implications for TcO_4^- sequestration, *Appl. Catal., B*, 192 (2016) 268–276.
- [40] G.V. Lowry, K.M. Johnson, Congener-specific dechlorination of dissolved PCBs by microscale and nanoscale zerovalent iron in a water/methanol solution, *Environ. Sci. Technol.*, 38 (2004) 5208–5216.
- [41] X. Wang, Z. Chen, X. Wang, Graphene oxides for simultaneous highly efficient removal of trace level radionuclides from aqueous solutions, *Sci. China Chem.*, 58 (2015) 1766–1773.
- [42] Y. Chen, W. Zhang, S. Yang, A. Hobiny, A. Alsaedi, X. Wang, Understanding the adsorption mechanism of Ni(II) on graphene oxides by batch experiments and density functional theory studies, *Sci. China Chem.*, 59 (2016) 412–419.
- [43] Y. Sun, S. Yang, Y. Chen, C. Ding, W. Cheng, X. Wang, Adsorption and desorption of U(VI) on functionalized graphene oxides: a combined experimental and theoretical study, *Environ. Sci. Technol.*, 49 (2015) 4255–4262.
- [44] X. Wang, S. Yang, W. Shi, J. Li, T. Hayat, X. Wang, Different interaction mechanisms of Eu(III) and $^{243}\text{Am(III)}$ with carbon nanotubes studied by batch, spectroscopy technique and theoretical calculation, *Environ. Sci. Technol.*, 49 (2015) 11721–11728.
- [45] Y. Zou, X. Wang, A. Khan, P. Wang, Y. Liu, A. Alsaedi, T. Hayat, X. Wang, Environmental remediation and application of nanoscale zero-valent iron and its composites for the removal of heavy metal ions: a review, *Environ. Sci. Technol.*, 50 (2016) 7290–7304.